High-fidelity entanglement of neutral atoms via a Rydberg-mediated single-modulated-pulse controlled-PHASE gate

Zhuo Fu [1,2] Peng Xu [1,3,*] Yuan Sun [4,†] Yang-Yang Liu,[1,2] Xiao-Dong He [1,3] Xiao Li,[1] Min Liu,[1] Run-Bing Li [1,3] Jin Wang [1,3] Liang Liu [4,‡] and Ming-Sheng Zhan [1,3,§]

[1]*State Key Laboratory of Magnetic Resonance and Atomic and Molecular Physics, Innovation Academy for Precision Measurement Science and Technology, Chinese Academy of Sciences, Wuhan 430071, China*
[2]*School of Physical Sciences, University of Chinese Academy of Sciences, Beijing 100049, China*
[3]*Wuhan Institute of Quantum Technology, Wuhan 430206, China*
[4]*Key Laboratory of Quantum Optics and Center of Cold Atom Physics, Shanghai Institute of Optics and Fine Mechanics, Chinese Academy of Sciences, Shanghai 201800, China*

The neutral atom platform has become an attractive choice to study the science of quantum information and quantum simulation, where intense efforts have been devoted to the entangling processes between individual atoms. A two-qubit controlled-PHASE gate via Rydberg blockade is one of the most essential elements. Recent theoretical studies have suggested the advantages of introducing nontrivial waveform modulation into the gate protocol, which is anticipated to improve its performance towards the next stage. We report our recent experimental results in realizing the two-qubit controlled-PHASE (C_Z) gate via single-modulated-pulse off-resonant modulated driving embedded in a two-photon transition for Rb atoms. It relies on a global driving laser pulse with a carefully calculated smooth waveform to gain the appropriate phase accumulations required by C_Z gate. Combining this C_Z gate with global microwave pulses, two-atom entanglement is generated with the raw fidelity of 0.945(6). After accounting for state preparation and measurement errors, we extract the entanglement operation fidelity to be 0.980(7). Our work features completing the C_Z gate operation within a single pulse to avoid shelved population in the Rydberg levels, thus demonstrating another promising route for realizing a high-fidelity two-qubit gate for the neutral atom platform.

I. INTRODUCTION

Neutral atoms have long been deemed as an essential platform in the study of quantum information [1–4] and quantum simulation [5–7], and recent rapid progress has revealed that cold atoms in optical traps serve as an ideal choice of qubits, where Rydberg blockade [8–10] serves as the backbone for the entangling processes between individual atoms. So far, intense efforts have been devoted to a wide range of experimental topics in this area, including the increment of number and type of qubits in array format [11,12], the enhancement of entangled state size [13], and the improvement of quantum gate performance [14–16]. These developments clearly demonstrate the promising potential of the neutral atom qubit and pave the way for future applications.

Amid many pressing tasks, an imminent challenge is to enhance the two-qubit gate fidelity towards the requirement of noisy intermediate-scale quantum technology (NISQ) under realistic experimental conditions [3,4,17]. There have been many proposals to improve the two-qubit gate fidelity against

different gate errors [18], including using adiabatic passage [19–22], using Rydberg dressing [23,24], using Rydberg antiblockade [25,26], using geometric quantum operations [27,28], using shaped analytic pulses [29,30], and so on. Also, many technical improvements have been made to improve the gate fidelity in the past decade, such as employing new Rydberg excitation laser setups to suppress or to eliminate intermediate state scattering [31–33], filtering laser phase noise with a high finesse cavity [34–36], cooling an atom down to the ground vibrational state in optical tweezers [37], and so on. However, the Rydberg-mediated two-qubit quantum gate demonstrated in current experiments [15,16,38], either C_Z gate or controlled-NOT gate, still yields less than satisfying fidelities [18,29]. One major reason for the infidelity is that atoms of superposition states are excited to the Rydberg state and are held on for a certain time, thus suffering from the severe decoherence between the ground state and the Rydberg state which is indicated by the ground-to-Rydberg-state Ramsey oscillations [22,39]. To realize the higher fidelity two-qubit quantum gate, it is necessary to reduce the Ramsey decoherence induced infidelity, such as increasing the ratio of Ramsey coherence time to gate time as done by [15].

Alternatively, it is possible to develop new schemes of the C_Z gate to avoid shelved Rydberg populations. Inspired by the controlled-PHASE gate protocol for single-photon ground-Rydberg transition with nontrivial smooth waveform

*etherxp@wipm.ac.cn
†yuansun@siom.ac.cn
‡liang.liu@siom.ac.cn
§mszhan@wipm.ac.cn

modulation methods [30], which provides the feasibility of driving both qubit atoms with the same control field, here we develop a method of the C_Z gate for two-photon transition via single-modulated-pulse off-resonant modulated driving (SORMD). Using global Rydberg excitation of two ^{87}Rb atoms within the Rydberg blockade region, the C_Z gate is realized via SORMD, where atoms are continuously driven in the ground-Rydberg transitions. We benchmark the gate fidelity by measuring the raw fidelity of two-atom entanglement to be $\mathcal{F} = 0.945(6)$. Correcting for state preparation and measurement (SPAM) errors, we extract the fidelity of entanglement operation to be $\mathcal{F}^c = 0.980(7)$.

The phase requirement of the C_Z gate in the two-qubit computational basis states $|00\rangle$, $|01\rangle$, $|10\rangle$, and $|11\rangle$ is

$$\phi_{00} - \phi_{01} - \phi_{10} + \phi_{11} = \pm\pi. \tag{1}$$

In our experiment, the SORMD method resorts to a specially tailored waveform of a 780 nm Rydberg-excitation laser to gain such phase accumulations under the presence of the Rydberg blockade, as illustrated in Fig. 1. The two-photon Rydberg-excitation configuration provides extra controlling laser and ac Stark shifts which significantly differ from the single-photon transition [30]. For experimental simplicity, we set a 480 nm Rydberg excitation laser as the constant driving laser while analyzing and calculating an amplitude modulated waveform for a 780 nm laser that starts and ends at zero. Without loss of generality, we choose a representation of the waveform in terms of a linear combination of basis polynomials:

$$\Omega_r(t)/2\pi = \sum_{\nu=1}^{4} \beta_\nu [b_{\nu,n}(t/T_g) + b_{n-\nu,n}(t/T_g)], \tag{2}$$

where $b_{\nu,n}$ is the νth Bernstein basis polynomial of degree n. The advantages of such a representation include its smoothness and compatibility with numerical optimization procedure and without a long tail. Under ideal conditions, the ultimate limit for the gate fidelity is the spontaneous lifetime of Rydberg levels and the residual thermal motion of qubit atoms. Here, for our experiment we choose the following set of parameters after optimization of the waveform: $\beta_1 = 206.4$ MHz, $\beta_2 = 90.1$ MHz, $\beta_3 = 300.5$ MHz, $\beta_4 = 97.98$ MHz, $n = 8$, intermediate detuning from $5P_{3/2}$ is $\Delta/2\pi = -5687$ MHz, pulse duration $T_g = 2$ μs, Rabi frequency of a 480 nm laser at 50 MHz, and the overall net two-photon detuning at $\delta/2\pi = 1.50$ MHz. Theoretically, the fidelity of two-atom entanglement is over 0.99 with these parameters.

II. EXPERIMENTAL PROCESS

The main experimental setup is shown in Fig. 2. Two ^{87}Rb atoms are trapped in two optical tweezers with a distance of 3.6(1) μm. Tightly focused 830 nm lasers generate the tweezers with the beam waist of 1.2(1) μm at the focal plane and these two traps are horizontally and symmetrically placed in the center of the global excitation laser beams. The temperature of single atoms is about 5.2 μk in a 50 μk trap after applying polarization-gradient cooling and adiabatic cooling. The qubits are encoded into the hyperfine ground
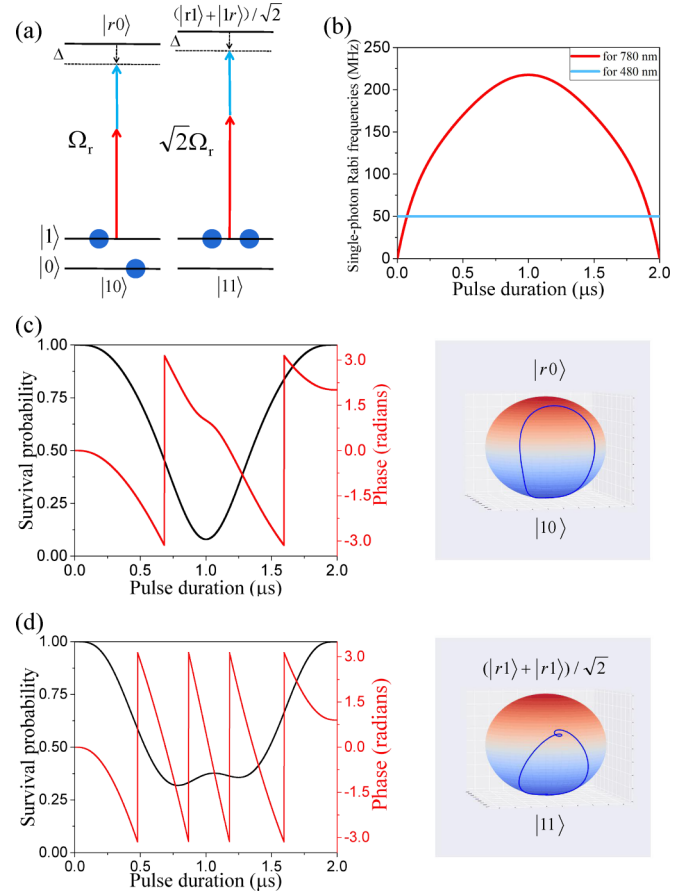

FIG. 1. Protocol of C_Z gate via single-modulated-pulse off-resonant modulated driving (SORMD). (a) Level diagram for two-photon Rydberg excitation. With Rydberg blockade, two atoms in $|11\rangle$ state will be excited to $(1/\sqrt{2})(|1r\rangle + |r1\rangle)$ with an enhanced effective Rabi frequency. (b) Calculated waveform of a SORMD pulse. SORMD only modulates the amplitude of a 780 nm laser with a waveform of a linear combination of Bernstein basis polynomials and keeps a 480 nm laser at a constant value. (c) The population and phase dynamics of $|01\rangle$ and $|10\rangle$ states. The population returns back with accumulated phase $\phi_{01} = \phi_{10} = 2.012$. (d) The population and phase dynamics of $|11\rangle$. The population also returns back but accumulates phase $\phi_{11} = 0.8997$. The Rydberg excitation laser is far off resonant for $|00\rangle$ state; thus ϕ_{00} can be ignored. After SORMD pulses, $\phi_{00} - \phi_{01} - \phi_{10} + \phi_{11} = -0.995\pi$.

state of the ^{87}Rb atom, with $|1\rangle = |5S_{1/2}, F = 2, m_F = 0\rangle$ and $|0\rangle = |5S_{1/2}, F = 1, m_F = 0\rangle$. We initialize all qubits by preparing atoms in $|1\rangle$ through an optical pumping procedure, with an efficiency of 99.2(2)%. The single-qubit operation is realized by 6.8 GHz microwave radiation and the Rabi oscillation frequency is about $2\pi \times 33$ kHz. We detect the atomic state by applying a resonant laser pulse which blows away atoms in state $|1\rangle$. The detection efficiency for state $|1\rangle$ is 99.3(2)% and atom preservation probability is 98.9(3)% for each trap. More details can be found in Appendixes A and B.

The Rydberg excitation from state $|1\rangle$ to state $|r\rangle = |79D_{5/2}, m_j = 5/2\rangle$ is realized by two-photon transition with counterpropagating 780 nm (σ^+) laser and 480 nm (σ^+) laser. The beam waist of the 780 nm laser is 7.8(3) μm
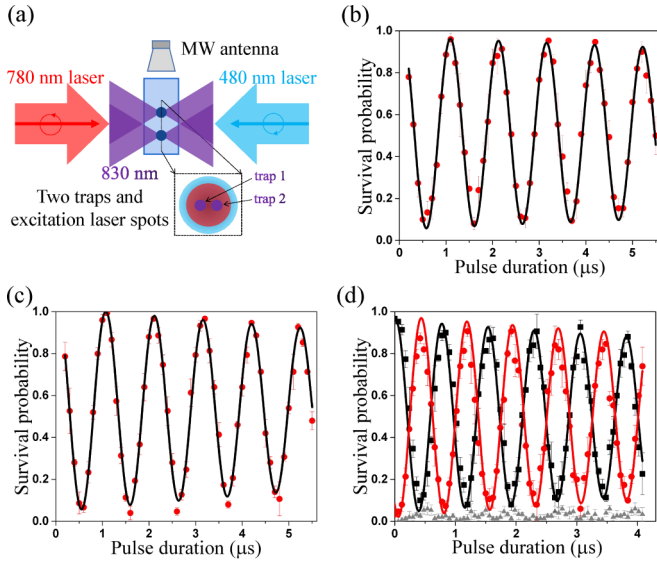
FIG. 2. Experimental setup and resonant two-photon ground-to-Rydberg-state Rabi oscillations. (a) Relevant lasers' configuration. Single-atom Rabi oscillations between $|1\rangle$ and $|r\rangle$ in trap 1 (b) and in trap 2 (c). Red dots are the measured survival probability of atoms after Rydberg excitation, which repeats 150 times. Black solid curves are damped sinusoidal fits, which give effective Rabi frequency of $2\pi \times 0.96(1)$ MHz and a decay time of 23(2) μs. (d) Two-atom collective Rabi oscillations between $|11\rangle$ and $(1/\sqrt{2})(|1r\rangle + |r1\rangle)$. Black squares are the measured probability of atoms surviving in both traps; red circles are the measured probability of atoms only surviving in one trap. At the same time gray triangles are the measured probability of atoms lost in both traps. The fitted Rabi frequency is $2\pi \times 1.35(2)$ MHz and a decay time of about 20 μs. Error bars in all figures are statistical and represent the standard deviation of the mean.

and the 480 nm laser is 8.3(5) μm. These two global excitation laser beams cover two traps as uniformly as possible. Several technical improvements have been made to achieve long-coherence Rabi oscillations of the ground-to-Rydberg-state transitions, such as reducing the Rydberg-excitation lasers' phase noise around 750 kHz for about 30 dB with a high-finesse cavity, suppressing Rydberg-excitation lasers' linewidth, stabilizing long term drift of laser frequencies, shielding stray electric field, and so on [36,39,40]. From the measured Rabi oscillations between $|1\rangle$ and $|r\rangle$ in Fig. 2(b), we deduce a $1/e$ decay time of $\tau = 23(2)$ μs and the effective Rabi frequency of $\Omega = 2\pi \times 0.96(1)$ MHz. By applying multiple Rydberg π pulses such as 1, 3, 5, and 7, we obtain Rydberg-excitation efficiency $P_{RE} = 98.9(3)\%$ and Rydberg-detection efficiency $P_{RD} = 88.9(9)\%$ [39]. Using a numerical simulation with qutip [41], we conclude that the decay of Rabi oscillation is mainly caused by the atom experienced intensity fluctuation of excitation lasers (see Appendix C). With the near-perfect Rydberg blockade, the excitation lasers globally couple two atoms from $|11\rangle$ to $|W\rangle = (1/\sqrt{2})(|1r\rangle + |r1\rangle)$. We observe an enhanced Rabi frequency of $\sqrt{2}\Omega \simeq 2\pi \times 1.35$ MHz [Fig. 2(d)]. Numerical simulation shows that the decay mechanism of collective excitation for two atoms is basically the same as the single-atom Rabi oscillation (Appendix C).
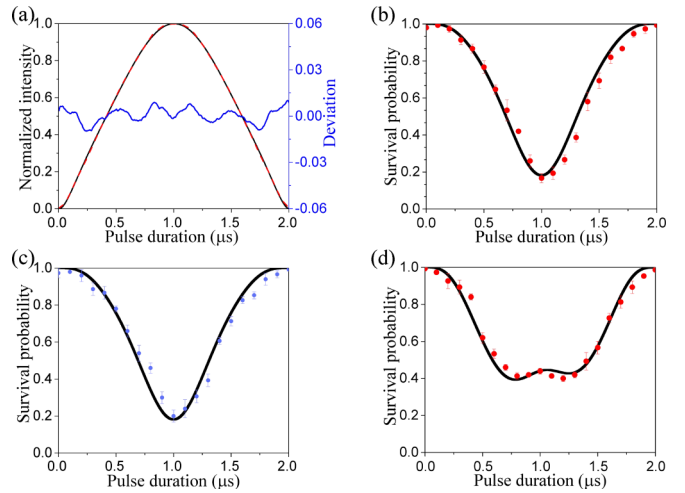

FIG. 3. Waveform of the 780 nm laser pulse and population evolutions of SORMD. (a) Calculated (solid black line) and generated (red dashed line) intensity waveform of a 780 nm pulse for SORMD. Blue line is the experimental deviation from the theoretical value. Population evolution of a single atom with $|1\rangle$ state in trap 1 (b) and in trap 2 (c) using the SORMD method. (d) Population evolution of $|11\rangle$ state using the SORMD method. The maximal single-photon Rabi frequency of the 780 nm laser and the 480 nm laser is adjusted to 217(2) MHz and 50.0(5) MHz, respectively. The circles are experimental results with 150 repetitions. Solid curves are theoretical predictions considering the 88.9% detection efficiency of the Rydberg state. Error bars in all figures are statistical and represent the standard deviation.

To implement SORMD, three critical things need to be done in advance. First, the single-photon Rabi frequencies of Rydberg-excitation lasers should be calibrated to the theoretical values as accurately as possible. For a 780 nm laser, different laser powers will cause different ac-Stark shifts of the Rydberg excitation peak. By linear fitting Rydberg peaks with laser powers, we can determine a 780 nm laser of 59.2 μW corresponds to $\Omega_{780} = 2\pi \times 217(2)$ MHz. Besides, we measure the Ramsey fringes of state $|0\rangle$ to $|1\rangle$ with different durations of 780 nm pulses in between two $\frac{\pi}{2}$ pulses; the calculated Ω_{780} from the shifted phases of Ramsey fringes agrees well with the previous result. Ω_{480} is then determined to be $2\pi \times 50.0(5)$ MHz of 120 mW laser power by measuring the Rabi oscillation frequency between $|1\rangle$ and $|r\rangle$ (see Appendix A). Second, the generated SORMD waveform of a 780 nm laser should be consistent with the calculated results. We modulate the amplitude of the rf signal, which is used to drive the acousto-optic modulator (AOM) via the input port of a mixer (Mini-circuits ZFM-3-S+). The generated waveform is in good agreement with the theoretical calculation and the deviation is less than 1%, as shown in Fig. 3(a). Third, the single-Rabi frequencies in two traps need to be balanced. We achieve the differences of Ω_{780} (Ω_{480}) between the two traps to be less than 0.5% (0.7%). This is done by fine-tuning the position of the 780 nm laser and the 480 nm laser with piezoelectric (Thorlabs, POLARIS-K1S2P) driven mirrors. When we finished these preparations, we excited the atoms with SORMD and measured the population of atoms in state $|1\rangle$ as Fig. 3 shows. It is worth noting that we have scanned the
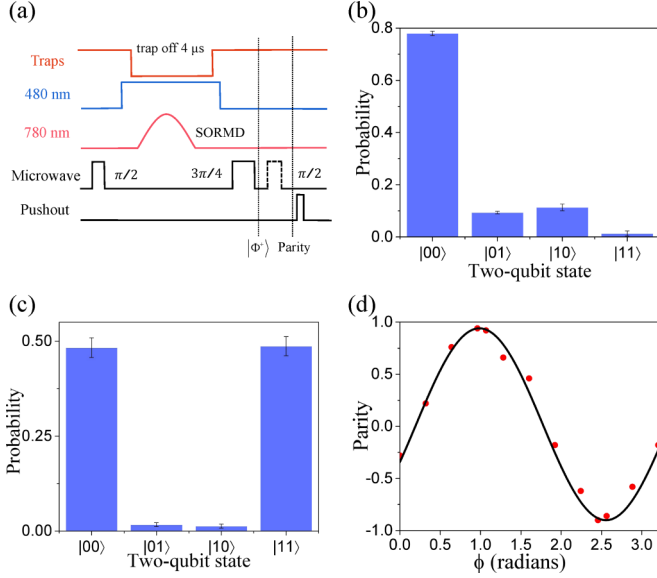
FIG. 4. C_Z gate realized by the SORMD method. (a) The pulse sequence for preparing Bell states $|\Phi^+\rangle$. After initialization, we first applied a global microwave $\frac{\pi}{2}$ pulse and then the SORMD pulse, which contains the modulated pulse of the 780 nm laser and a square pulse of the 480 nm laser. Thirdly, we apply a global microwave $\frac{3\pi}{4}$ pulse. At last, the pushout pulse is used to blow away the atoms in state $|1\rangle$. (b) The measured population of the two-qubit state without a SORMD pulse. (c) Bell state population. Raw measurements give $(P_{00} + P_{11})/2 = 0.485(4)$. (d) The measured amplitude of parity oscillation is 0.92(1) and the raw fidelity of the Bell state is $F_{\text{Bell}} = 0.485 + 0.46 = 0.945(6)$.

TABLE I. Calibrating the fidelity of $(1/\sqrt{2})(|00\rangle+|11\rangle)$ generated by SORMD.

	Raw data	Lower bound	Corrected
Population	0.970	0.950	0.990
Coherence	0.920	0.920	0.970
State fidelity	0.945	0.935	0.980

pushout beam to set a lower bound of the Bell state population as $(P_{00} + P_{11})/2 \geqslant 0.475(4)$. To evaluate the actual fidelity of SORMD operation, it is necessary to further correct the SPAM errors. By designing different experiments to decouple errors of state preparation, state transition, and state detection, we carefully calibrate the SPAM error to be 2.6(4)% per atom (see Appendix B). Referring to the correcting methods of SPAM errors in [15], the Bell state fidelity is corrected as $\mathcal{F}^c = 0.980(7)$ (see Appendix D). The detailed value of Bell state population and coherence after correcting SPAM are listed in Table I. The infidelity of the SORMD generated C_Z gate mainly arises from the off-resonant scattering of the intermediate state and the imbalance of Rabi frequencies between two atoms. These defects will be improved in follow-on work by using Rydberg excitation lasers which couple the intermediate state of longer lifetimes and by cooling atoms down to a lower temperature.

excitation frequency due to the two-photon detuning $\delta/2\pi = 1.50$ MHz. Compared with the theoretical calculations, the evolution of the population curves is within expectations and the imperfections may be caused by the excitation frequency and single-photon Rabi frequencies' fluctuations in two traps.

Finally, we illustrate that SORMD can realize the C_Z gate by using it to create Bell states $|\Phi^+\rangle = (1/\sqrt{2})(|00\rangle + |11\rangle)$ with the pulse sequence shown in Fig. 4. We first initialize atoms to the state $|11\rangle$ and apply a global microwave $\frac{\pi}{2}$ pulse to prepare them in state $(1/2)(|00\rangle\text{-}i|01\rangle\text{-}i|10\rangle\text{-}|11\rangle)$. Then we apply the 2 μs SORMD and a global microwave $\frac{3\pi}{4}$ pulse to produce the Bell state $|\Phi^+\rangle$. Figure 4(c) shows the experimental data of Bell state population, which gives $(P_{00} + P_{11})/2 = 0.485(4)$. In addition, we scan the phase of the last global microwave $\frac{3\pi}{4}$ pulse to compensate for the relative phase of the C_Z gate. As a comparison, we repeat the same pulse sequence, but without SORMD, which generates population in four states of 0.78(1), 0.093(5), 0.11(1), and 0.013(9). The population difference in Figs. 4(b) and 4(c) clearly shows that SORMD creates a C_Z gate. To benchmark the gate fidelity, we measure the coherence of Bell states as shown in Fig. 4(d) by applying a global microwave $\frac{\pi}{2}$ pulse with a variable phase. The measured parity amplitude is $C = 0.460(5)$. So the raw fidelity of the Bell state is $\mathcal{F} = 0.485 + 0.46 = 0.945(6)$.

In the experimental process, atoms lost due to background gas collision or finite atomic temperature are also classified as in state $|1\rangle$, which will cause an overestimation of the population. Thus we measure the population in which we disable the

III. CONCLUSION AND DISCUSSION

In conclusion, we have experimentally implemented a category of the two-qubit controlled-PHASE gate based upon Rydberg blockade effects. In our method, atoms are continuously driven in the ground-Rydberg transitions to make full use of long-coherence Rabi oscillations instead of the shorter-coherence Ramsey oscillations. We are also looking forward to a few other future refinements, including the search for a faster gate operation, further suppression of population leakage, stronger robustness against environmental noises, and a more user-friendly parameter setting. An error correction mechanism [42] for our gate protocol is also part of the long-term goal. Our aim is to help the translation of high-quality ground-Rydberg coherence into the high-fidelity controlled-PHASE gate via the Rydberg blockade effect.
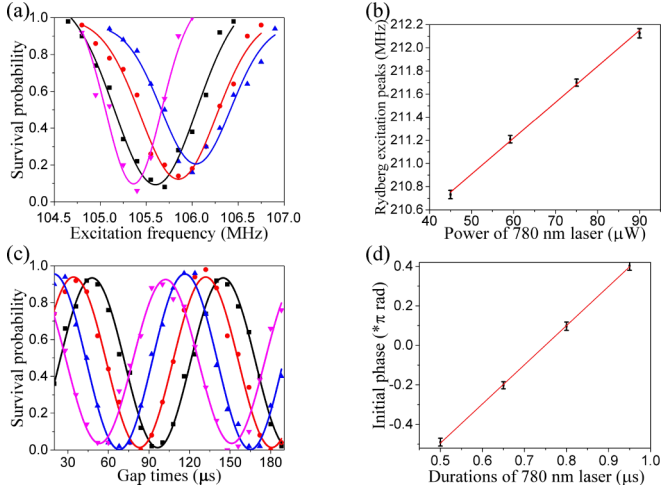
FIG. 5. Measurement of single-photon Rabi frequencies of 780 nm. (a) Experimental data of Rydberg excitation peaks at different 780 nm powers. (b) Linear fitting of the excitation peaks and powers, which gives $k = 0.031(1)$. (c) Ramsey fringes between ground states with 0.5 μs, 0.65 μs, 0.8 μs, and 0.95 μs durations of 780 nm pulses in between two $\pi/2$ microwave pulses. (d) Linear fitting the initial phases of Ramsey fringes and durations of 780 nm pulses gives $k1 = 1.98(2)$.

APPENDIX A: CALIBRATING SINGLE-PHOTON RABI FREQUENCIES

To drive the atoms to evolve as calculated and to accumulate appropriate phases when implementing the SORMD method, we should measure and adjust the single-photon Rabi frequencies of 780 nm (Ω_{780}) laser and 480 nm (Ω_{480}) laser to the predetermined values. First, we calibrate Ω_{780} with two methods. One method is to measure the Rydberg excitation peaks at different 780 nm laser powers and make a linear fitting of these peaks, which gives a slope k. In addition, to reduce the broadening of the excitation peaks, we measure the peaks with a 3π Rydberg pulse. Since the ac-Stark shift of state $|1\rangle$ caused by the 780 nm excitation laser is proportional to the square of single-photon Rabi frequencies of 780 nm, the relationship between Ω_{780} and k can be expressed as $\Omega_{780} = \sqrt{4\Delta k P_0}$, where P_0 represents the power of the 780 nm laser and $\Delta/2\pi = -5687(10)$ MHz. Fures 5(a) and 5(b) show our experimental data and give $k = 0.031(1)$, so $\Omega_{780}/2\pi = 205(3)$ MHz. Then we can adjust the power of the 780 nm laser to get the required value of $\Omega_{780}/2\pi = 217.6$ MHz.

The other method is to measure the Ramsey fringes of state $|1\rangle$ to $|0\rangle$ with different durations of 780 nm pulses in between two $\pi/2$ pulses [see Fig. 5(c)]. The scale factor $k1$ between initial phases of the fringes and durations of 780 nm pulses implies the difference of ac-Stark shifts between states $|0\rangle$ and $|1\rangle$. The relationship is expressed as

$$\frac{\Omega_{780}^2}{2\pi \times 4\Delta} + \frac{\Omega_{780}^2}{2\pi \times 4(\Delta + 6834.7)} = k1. \qquad (A1)$$

Figure 5(d) shows the linear fitting of initial phases and durations from which we calculate $\Omega_{780}/2\pi = 204(1)$ MHz. The
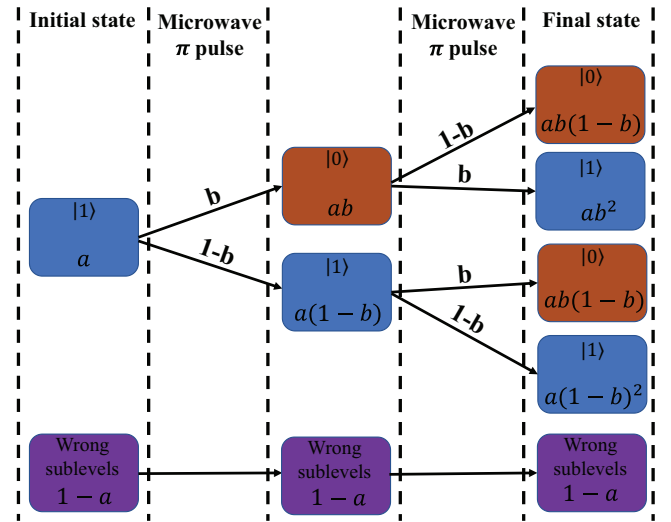

FIG. 6. Probability distribution for microwave transition. The first column represents the initial states and probabilities after the optical pumping process. The second column shows the possible atomic states in trap and probabilities after we apply a microwave π pulse. In the last column, we list all the possible states and probabilities after two microwave π pulses.

results obtained by the two methods agree well with each other.

Second, $\Omega_{480}/2\pi = 49.9(8)$ MHz is deduced from the relation

$$\Omega = \frac{\Omega_{780} \times \Omega_{480}}{2\Delta}, \qquad (A2)$$

where $\Omega/2\pi = 0.954(7)$ MHz is fitted from Rabi oscillation. In conclusion, the error of calibrating single-photon Rabi frequencies with these methods is within 2%.

APPENDIX B: STATE PREPARATION AND MEASUREMENT (SPAM) ERRORS

The SPAM errors include atom preservation error, state measurement error, and optical pumping error. Since these three errors are intertwined with each other, they should be solved one by one. Atom preservation errors in traps are caused by background collision and finite atomic temperature. We can estimate this error by collecting the statistics of atoms in the trap without a push-out pulse. In our experiment, the error of the atom loss in a single trap is 1.1(3)%. State measurement errors can be evaluated by counting the residual atoms after pushing out atoms in $F = 2$. Considering the atom preservation efficiency, that state measurement error is 0.7(2)% per qubit in our experiment.

We have designed two experiments with microwave pulses to estimate the optical pumping efficiency (denoted as a) and microwave transition efficiency (denoted as b) in a single trap. First, we apply a microwave π pulse after the optical pumping process and then apply a push-out pulse; there are 98.0(3)% atoms still in the trap at last. The state transition process and probabilities are illustrated in Fig. 6: the probability of atoms in state $|1\rangle$ transferred into state $|0\rangle$ is $P_1 = ab$, the probability of atoms still in state $|1\rangle$ due to imperfect microwave transi-
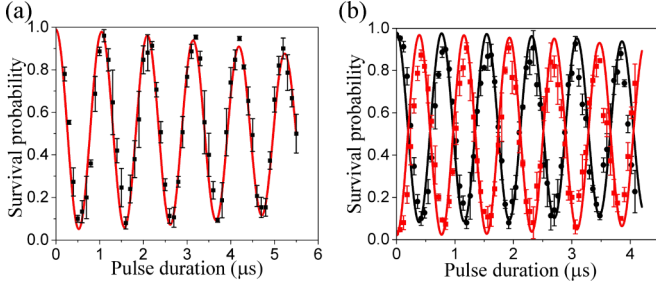
FIG. 7. Numerical simulation for single-atom ground-Rydberg Rabi oscillation and two-atoms collective excitation with qutip. (a) Red line represents the simulated data of single-atom Rabi oscillation and red squares are experimental data. Main parameters are set as $\Omega_{780}/2\pi = 217$ MHz and $\Omega_{480}/2\pi = 50$ MHz and intermediate detuning of $\Delta/2\pi = -5687$ MHz. (b) Numerical simulation for two-atoms collective excitation. Black and red lines are simulated data and represent the survival probability of state $|11\rangle$ and state $(1/\sqrt{2})(|1r\rangle + |r1\rangle)$, respectively. Black dots and red squares are corresponding experimental data. Main parameters are the same as those of a single atom in (a).

tion is $P_2 = a(1 - b)$, and the probability of atoms in other incorrect magnetic sublevels is $P_3 = (1 - a)$. The probability of atoms still in the trap can be expressed as

$$\{ab + [a(1 - b) + 1 - a] \times (1 - 0.993)\} \times 0.989 = 0.980. \tag{B1}$$

Secondly, after the optical pumping process, we apply two microwave π pulses and detect the atoms with a push-out laser; there are only 0.8(2)% of atoms remaining in the trap. The probability of atoms in state $|1\rangle$ returning to the original state after two microwave π pulses is $P_4 = ab^2$, the probability of atoms in state $|1\rangle$ transferred into state $|0\rangle$ is $P_5 = 2ab(1 - b)$, the probability of atoms in state $|1\rangle$ not participating in the evolution is $P_6 = a(1 - b)^2$, and the probability of atoms in other wrong sublevels is $P_3 = (1 - a)$. The probability of left atoms is

$$\{2ab(1 - b) + [ab^2 + a(1 - b)^2 + 1 - a]$$
$$\times (1 - 0.993)\} \times 0.989$$
$$= 0.08. \tag{B2}$$

According to Eqs. (B1)and (B2), we can solve that the optical pumping efficiency is 99.2(2)% [which implies the optical pumping error is 0.8(2)%] and the microwave transition efficiency is 99.9(1)%.

In summary, the SPAM error is 2.6(4)% per qubit in our system.

APPENDIX C: NUMERICAL SIMULATION

To evaluate the decay mechanism of ground-Rydberg Rabi oscillation in our system, we carry out the numerical simulation with qutip. Figure 7(a) shows a typical result for single-atom ground-Rydberg Rabi oscillation. Red line and red squares represent simulated data and experimental data, respectively. We set single-photon Rabi frequencies of $\Omega_{780}/2\pi = 217$ MHz and $\Omega_{480}/2\pi = 50$ MHz and intermediate detuning of $\Delta/2\pi = -5687$ MHz. The numerical model mainly considers the effect of effective Rabi frequency fluctuation (~2%), random Doppler shifts (~17 kHz), scattering from the intermediate state, and detection efficiency for Rydberg state atoms (~90%). Without adjusting any other parameters, the simulated data agree well with the experimental data. We can conclude that the fluctuation of effective Rabi frequency is the main reason for the decay of Rabi oscillation. This fluctuation comes from the intensity fluctuation of excitation lasers and atom distribution in the inhomogeneous light field. Figure 7(b) shows the numerical simulation for two-atoms collective excitation; related parameters are the same as those in single-atom simulation. Black dots and red squares are experimental data; black line and red line represent the simulated probability of state $|11\rangle$ and state $(1/\sqrt{2})(|1r\rangle + |r1\rangle)$, respectively. We observe good agreement between numerical simulation and experimental results and this implies a near-perfect Rydberg blockade between two atoms. More importantly, we can conclude that the decay mechanism of two-atoms collective excitation is basically the same as the single-atom Rabi oscillation in our system.

APPENDIX D: BELL STATE FIDELITY

According to the method in Ref.[15], the measured fidelity is related to the corrected fidelity:

$$\mathcal{F} = P \times \mathcal{F}^c + (1 - P) \times \mathcal{F}^{\text{false}}. \tag{D1}$$

Here, $P = (1 - 2.6\%)^2$ denotes the probability to correctly initialize and measure two qubits. $\mathcal{F}^{\text{false}}$ denotes the false contribution to the F when SPAM error occurs, where $\mathcal{F}^{\text{false}} \approx 15\%$ in the correction of Bell state population and $\mathcal{F}^{\text{false}} = 0$ in the correction of parity oscillation. Due to the state measurement method in our experiment, the lost atoms will be classified as state $|1\rangle$, which will cause the overestimation of state $|11\rangle$ in the Bell state population. After correcting this overestimation, we get the lower bound on the measured Bell state populations, $(p_{00} + p_{11})/2 \geqslant [0.485 \times 2 - (1 - 0.98)/2] = 0.475(4)$, therefore giving a lower bound on the corrected populations: $(p_{00}^c + p_{11}^c)/2 \geqslant 0.495(5)$. In addition, the amplitude of the parity oscillation $C = 0.460(5)$ is related to the corrected amplitude according to $C = P \times C^c$. We obtain the corrected amplitude $C^c = 0.485(6)$. Finally, the SPAM-corrected Bell state fidelity is $\mathcal{F}^c = (p_{00}^c + p_{11}^c + C^c)/2 = 0.980(7)$.

[1] M. Saffman, T. G. Walker, and K. Mølmer, Quantum information with Rydberg atoms, Rev. Mod. Phys. **82**, 2313 (2010).

[2] M. Saffman, Quantum computing with atomic qubits and Rydberg interactions: Progress and challenges, J. Phys. B: At., Mol., Opt. Phys. **49**, 202001 (2016).

[3] L. Henriet, L. Beguin, A. Signoles, T. Lahaye, A. Browaeys, G.-O. Reymond, and C. Jurczak, Quantum computing with neutral atoms, Quantum **4**, 327 (2020).

[4] M. Morgado and S. Whitlock, Quantum simulation and computing with Rydberg-interacting qubits, AVS Quantum Sci. **3**, 023501 (2021).

[5] A. Browaeys and T. Lahaye, Many-body physics with individually controlled Rydberg atoms, Nat. Phys. **16**, 132 (2020).

[6] P. Scholl, M. Schuler, H. J. Williams, A. A. Eberharter, D. Barredo, K.-N. Schymik, V. Lienhard, L.-P. Henry, T. C. Lang, T. Lahaye, A. M. Läuchli, and A. Browaeys, Quantum simulation of 2D antiferromagnets with hundreds of Rydberg atoms, Nature (London) **595**, 233 (2021).

[7] S. Ebadi, T. T. Wang, H. Levine, A. Keesling, G. Semeghini, A. Omran, D. Bluvstein, R. Samajdar, H. Pichler, W. W. Ho, S. Choi, S. Sachdev, M. Greiner, V. Vuleti, and M. D. Lukin, Quantum phases of matter on a 256-atom programmable quantum simulator, Nature (London) **595**, 227 (2021).

[8] D. Jaksch, J. I. Cirac, P. Zoller, S. L. Rolston, R. Côté, and M. D. Lukin, Fast Quantum Gates for Neutral Atoms, Phys. Rev. Lett. **85**, 2208 (2000).

[9] L. Isenhower, E. Urban, X. L. Zhang, A. T. Gill, T. Henage, T. A. Johnson, T. G. Walker, and M. Saffman, Demonstration of a Neutral Atom Controlled-NOT Quantum Gate, Phys. Rev. Lett. **104**, 010503 (2010).

[10] T. Wilk, A. Gaëtan, C. Evellin, J. Wolters, Y. Miroshnychenko, P. Grangier, and A. Browaeys, Entanglement of Two Individual Neutral Atoms Using Rydberg Blockade, Phys. Rev. Lett. **104**, 010502 (2010).

[11] A. Kumar, T. Y. Wu, F. Giraldo, and D. S. Weiss, Sorting ultracold atoms in a three-dimensional optical lattice in a realization of Maxwell's demon, Nature (London) **561**, 83 (2018).

[12] D. Ohl de Mello, D. Schäffner, J. Werkmann, T. Preuschoff, L. Kohfahl, M. Schlosser, and G. Birkl, Defect-Free Assembly of 2D Clusters of More Than 100 Single-Atom Quantum Systems, Phys. Rev. Lett. **122**, 203601 (2019).

[13] A. Omran, H. Levine, A. Keesling, G. Semeghini, T. T. Wang, S. Ebadi, H. Bernien, A. S. Zibrov, H. Pichler, S. Choi, J. Cui, M. Rossignolo, P. Rembold, S. Montangero, T. Calarco, M. Endres, M. Greiner, V. Vuletić, and M. D. Lukin, Generation and manipulation of Schrödinger cat states in Rydberg atom arrays, Science **365**, 570 (2019).

[14] M. Ebert, M. Kwon, T. G. Walker, and M. Saffman, Coherence and Rydberg Blockade of Atomic Ensemble Qubits, Phys. Rev. Lett. **115**, 093601 (2015).

[15] H. Levine, A. Keesling, G. Semeghini, A. Omran, T. T. Wang, S. Ebadi, H. Bernien, M. Greiner, V. Vuletić, H. Pichler, and M. D. Lukin, Parallel Implementation of High-Fidelity Multiqubit Gates with Neutral Atoms, Phys. Rev. Lett. **123**, 170503 (2019).

[16] T. M. Graham, M. Kwon, B. Grinkemeyer, Z. Marra, X. Jiang, M. T. Lichtman, Y. Sun, M. Ebert, and M. Saffman, Rydberg-Mediated Entanglement in a Two-Dimensional Neutral Atom Qubit Array, Phys. Rev. Lett. **123**, 230501 (2019).

[17] D. S. Weiss and M. Saffman, Quantum computing with neutral atoms, Phys. Today **70**(7), 44 (2017).

[18] X. L. Zhang, A. T. Gill, L. Isenhower, T. G. Walker, and M. Saffman, Fidelity of a Rydberg-blockade quantum gate from simulated quantum process tomography, Phys. Rev. A **85**, 042310 (2012).

[19] D. D. B. Rao and K. Mølmer, Robust Rydberg-interaction gates with adiabatic passage, Phys. Rev. A **89**, 030301(R) (2014).

[20] I. I. Beterov, M. Saffman, E. A. Yakshina, D. B. Tretyakov, V. M. Entin, S. Bergamini, E. A. Kuznetsova, and I. I. Ryabtsev, Two-qubit gates using adiabatic passage of the Stark-tuned Förster resonances in Rydberg atoms, Phys. Rev. A **94**, 062307 (2016).

[21] I. I. Beterov, G. N. Hamzina, E. A. Yakshina, D. B. Tretyakov, V. M. Entin, and I. I. Ryabtsev, Adiabatic passage of radio-frequency-assisted Förster resonances in Rydberg atoms for two-qubit gates and the generation of Bell states, Phys. Rev. A **97**, 032701 (2018).

[22] M. Saffman, I. I. Beterov, A. Dalal, E. J. Páez, and B. C. Sanders, Symmetric Rydberg controlled-z gates with adiabatic pulses, Phys. Rev. A **101**, 062309 (2020).

[23] T. Keating, R. L. Cook, A. M. Hankin, Y.-Y. Jau, G. W. Biedermann, and I. H. Deutsch, Robust quantum logic in neutral atoms via adiabatic Rydberg dressing, Phys. Rev. A **91**, 012337 (2015).

[24] A. Mitra, M. J. Martin, G. W. Biedermann, A. M. Marino, P. M. Poggi, and I. H. Deutsch, Robust Mølmer-Sørensen gate for neutral atoms using rapid adiabatic Rydberg dressing, Phys. Rev. A **101**, 030301(R) (2020).

[25] X.-F. Shi, Rydberg Quantum Gates Free from Blockade Error, Phys. Rev. Applied **7**, 064017 (2017).

[26] S.-L. Su and W. Li, Dipole-dipole-interaction–driven antiblockade of two Rydberg atoms, Phys. Rev. A **104**, 033716 (2021).

[27] M. Li, F.-Q. Guo, Z. Jin, L.-L. Yan, E.-J. Liang, and S.-L. Su, Multiple-qubit controlled unitary quantum gate for Rydberg atoms using shortcut to adiabaticity and optimized geometric quantum operations, Phys. Rev. A **103**, 062607 (2021).

[28] F.-Q. Guo, J.-L. Wu, X.-Y. Zhu, Z. Jin, Y. Zeng, S. Zhang, L.-L. Yan, M. Feng, and S.-L. Su, Complete and nondestructive distinguishment of many-body Rydberg entanglement via robust geometric quantum operations, Phys. Rev. A **102**, 062410 (2020).

[29] L. S. Theis, F. Motzoi, F. K. Wilhelm, and M. Saffman, High-fidelity Rydberg-blockade entangling gate using shaped, analytic pulses, Phys. Rev. A **94**, 032306 (2016).

[30] Y. Sun, P. Xu, P.-X. Chen, and L. Liu, Controlled Phase Gate Protocol for Neutral Atoms Via Off-Resonant Modulated Driving, Phys. Rev. Applied **13**, 024059 (2020).

[31] K. M. Maller, M. T. Lichtman, T. Xia, Y. Sun, M. J. Piotrowicz, A. W. Carr, L. Isenhower, and M. Saffman, Rydberg-blockade controlled-NOT gate and entanglement in a two-dimensional array of neutral-atom qubits, Phys. Rev. A **92**, 022336 (2015).

[32] Y. Y. Jau, A. M. Hankin, T. Keating, I. H. Deutsch, and G. W. Biedermann, Entangling atomic spins with a Rydberg-dressed spin-flip blockade, Nat. Phys. **12**, 71 (2016).

[33] C. J. Picken, R. Legaie, K. McDonnell, and J. D. Pritchard, Entanglement of neutral-atom qubits with long ground-Rydberg coherence times, Quantum Sci. Technol. **4**, 015011 (2018).

[34] H. Levine, A. Keesling, A. Omran, H. Bernien, S. Schwartz, A. S. Zibrov, M. Endres, M. Greiner, V. Vuletić, and M. D. Lukin, High-Fidelity Control and Entanglement of Rydberg-Atom Qubits, Phys. Rev. Lett. **121**, 123603 (2018).

[35] S. de Léséleuc, D. Barredo, V. Lienhard, A. Browaeys, and T. Lahaye, Analysis of imperfections in the coherent optical excitation of single atoms to Rydberg states, Phys. Rev. A **97**, 053803 (2018).

[36] Y.-Y. Liu, Z. Fu, P. Xu, X.-D. He, J. Wang, and M.-S. Zhan, Spectral filtering of dual lasers with a high-finesse length-tunable cavity for rubidium atom Rydberg excitation, Chin. Phys. B **30**, 074203 (2021).

[37] I. S. Madjarov, J. P. Covey, A. L. Shaw, J. Choi, A. Kale, A. Cooper, H. Pichler, V. Schkolnik, J. R. Williams, and M. Endres, High-fidelity entanglement and detection of alkaline-earth Rydberg atoms, Nat. Phys. **16**, 857 (2020).

[38] Y. Zeng, P. Xu, X.-D. He, Y.-Y. Liu, M. Liu, J. Wang, D. J. Papoular, G. V. Shlyapnikov, and M.-S. Zhan, Entangling Two Individual Atoms of Different Isotopes via Rydberg Blockade, Phys. Rev. Lett. **119**, 160502 (2017).

[39] Y.-Y. Liu, Y. Sun, Z. Fu, P. Xu, X. Wang, X.-D. He, J. Wang, and M.-S. Zhan, Infidelity Induced by Ground-Rydberg Decoherence of the Control Qubit in a Two-Qubit Rydberg-Blockade Gate, Phys. Rev. Applied **15**, 054020 (2021).

[40] Y. Zeng, K.-P. Wang, Y.-Y. Liu, X.-D. He, M. Liu, P. Xu, J. Wang, and M.-S. Zhan, Stabilizing dual laser with a tunable high-finesse transfer cavity for single-atom Rydberg excitation, J. Opt. Soc. Am. B **35**, 454 (2018).

[41] J. R. Johansson, P. D. Nation, and F. Nori, Qutip 2: A python framework for the dynamics of open quantum systems, Comput. Phys. Commun. **184**, 1234 (2013).

[42] D. Crow, R. Joynt, and M. Saffman, Improved Error Thresholds for Measurement-Free Error Correction, Phys. Rev. Lett. **117**, 130503 (2016).